On the relationship of energetic particle precipitation and mesopause temperature

Florine Enengl[1,2], Noora Partamies[2,3], Nickolay Ivchenko[1], and Lisa Baddeley[2,3]

[1]KTH Royal Insitute of Technology, Stockholm, Sweden
[2]The University Centre in Svalbard, Norway
[3]Birkeland Centre for Space Science, Norway

Correspondence: Florine Enengl (florine@kth.se)

Abstract. Energetic Particle Precipitation (EPP) has the potential to change the neutral atmospheric temperature at the mesopause region. Recent results, however, are inconsistent leaving the mechanism and the actual effect still unresolved. Here we have searched for electron precipitation events and investigated a possible correlation between D region electron density enhancements and simultaneous neutral temperature changes. The rotational temperature of the exited hydroxyl (OH) molecules is retrieved from the spectrum of the OH airglow. The electron density is monitored by the EISCAT Svalbard radar from the International Polar Year (IPY) in 2007–2008, when the EISCAT Svalbard radar was run continuously, until February 2019. Particle precipitation events are characterized by rapid increases in electron density by a factor of 4 at an altitude range of 80–95 km, which overlaps with the nominal altitude of the OH airglow layer. The OH airglow measurements and the electron density measurements are co-located. Most of our 8 electron precipitation events are associated with a temperature decrease of 10–50 K. Only one event was related to temperature change less than 10 K. We interpret the results in terms of the change in the chemical composition in the mesosphere. Due to EPP ionisation the population of excited OH at the top of the airglow layer decreases. As a consequence, the airglow peak height changes and the temperatures are probed at lower altitudes, providing inconsistent temperature responses. This is in agreement with conclusions of earlier studies, but is, for the first time, constructed from electron precipitation measurements as opposed proxies. The EPP related temperature change recovers very fast, typically within 30 minutes. We therefore further conclude that this type of particle precipitation events would only have a significant impact on the longer-term heat balance in the mesosphere if the lifetime of the precipitation was much longer than that of a typical EPP event found in this study.

1 Introduction

Space weather phenomena can affect the dynamics and the heat balance of the atmosphere by depositing energy in the form of energetic particle precipitation. In particular, investigating the mesopause region (at 80–100 km), the boundary between the mesosphere and the thermosphere (Andrews, 2010), is important. At the lower boundary of the ionosphere and the upper

boundary of the neutral atmosphere, the behaviour of neutral gas and ionized particles differ, which is why complex interactions between dynamics, photochemistry, heating and transport mechanisms take place and the atmospheric energy budget can be

25 altered.

Several studies have investigated the effects of energetic particle precipitation (EPP) on neutral temperatures in the mesopause region. Nesse Tyssøy et al. (2010) compared particle precipitation observed by NOAA POES satellites with neutral temperatures derived from the TIMED satellite. They used a dataset of 80 days within May–June and October–November in 2003 over the northern hemisphere. Temperature profiles were averaged over all local time hours for four flux levels of precipitating

30 energetic protons. A temperature increase of about 40 K at 115–120 km associated with strong fluxes of 80–250 keV protons in October–November was found. The strongest temperature increase of 15–20 K in May–June at the altitudes of 110–115 km was reported due to high fluxes of 30–80 keV protons. As particle precipitation events change the Pedersen conductivity, Joule heating may contribute to the increase in temperature at these altitudes. Further down in the atmosphere, at 85–90 km, only a minor cooling of 3–4 K during periods of high Kp values was observed due to precipitation of 250–800 keV protons (an

35 intense solar proton event).

The rotational hydroxyl (OH) airglow temperature was observed during six nights of the austral winter in 2008 by Suzuki et al. (2010). These nights were selected to include high auroral activity and clear weather. In their study, the temperature was derived from spectra recorded at Syowa Station in Antarctica by a high-sensitivity spectrometer. During only one of these nights (27–28 March 2008), an increase in the temperature of 10 K over a time period of 15 minutes was observed. Furthermore, a

40 decrease in the relative intensity of the OH(8–4) Q branch of ∼23% was found by comparing the pre-EPP level to that half an hour after the deepest magnetic deflection. No such coherent behaviour was seen during the other nights. Suzuki et al. (2010) suggested a relationship between EPP and the OH temperature based on measured disturbances in the horizontal magnetic field and variations in the cosmic radio noise absorption (CNA) over the course of several hours of activity. The average energy of the precipitating electrons during this night reached 10–20 keV. They discussed different mechanisms for causing the change

45 in the temperature. Joule heating was concluded to not contribute much, as the estimated heating rate required to explain the observed temperature increase at the mesopause height was three orders of magnitude higher than earlier particle precipitation observations suggested. Direct particle heating, on the other hand, is produced by precipitating particles colliding with the atmospheric neutrals. This heating process is dependent on the incident particle energy and their deposition altitude. Similarly to the Joule heating, the authors estimated the energy deposition rate of EPP at the mesopause height, and concluded that the

50 high-energy particle flux required to explain the temperature change was unrealistically high. Atmospheric gravity waves were also excluded, as the intensity of the OH airglow and the rotational temperature did not show a positive correlation, which is characteristic for dynamics driven conditions, as described and modelled by Cho and Shepherd (2006). Suzuki et al. (2010) further discussed the possibility of a change in the height distribution of the OH airglow emission during auroral events. The initial profile of OH volume emission rates retrieved by the SABER instrument onboard the TIMED satellite was compared to

55 an example of the disturbed layer. The comparison showed a decrease in the upper part of the disturbed layer as the thickness of the OH layer had decreased by 20%. If a change in the height distribution of the OH airglow emission occurred during an

auroral event, an increase in temperature is not necessarily observed, as the outcome would also depend on the temperature gradient in the mesosphere.

The connection between the geomagnetic activity and the long-term temperature at the mesopause region during the solar
60 cycle 23 and 24 was studied by Gavrilyeva and Ammosov (2018). The OH rotational temperature was measured by the ground-based infrared spectrograph at Maimaga station (63°N,129.5°E), and ascribed to an altitude of 87 km, which is commonly assumed to be the peak height of the OH layer. The seasonally averaged temperatures from 1999 to 2015 were included in the analysis. The results showed that the mesopause temperature from October to February is about 10 K higher during the years with high solar activity (Ap > 8) than during low activity years (Ap ≤ 8). A solar activity dependence of OH airglow
65 temperatures was also reported by Holmen et al. (2014). They concluded on a temperature change of about 4 K per 100 solar flux units (SFU) of the F10.7 radio flux. The question on the detailed relationship of EPP and the mesopause temperature was still left open.

The purpose of this study is to characterize the effects of the EPP on the mesopause temperature in more detail, on a larger set of events, in higher temporal resolution and using co-located measurements of precipitating electrons and the mesospheric
70 temperature. The instrumentation is further described in section 2. Section 3 outlines the data used in this study, as well as the analysis of the EISCAT Svalbard Radar data. Finally, the results are shown and discussed in sections 4 and 5. The conclusions of the effects of the EPP on the mesopause temperature are summarized in section 6.

2   Instrumentation

Following Cresswell-Moorcock et al. (2013) we use the European Incoherent Scatter Scientific Association (EISCAT) radar
75 data to identify electron precipitation events as electron density enhancements. Simultaneous and co-located neutral temperature measurements are determined using the spectrometer measurements of the OH airglow. The derived rotational OH temperature is taken as the neutral temperature of the mesopause region, assuming that the excited OH molecules are in thermal equilibrium with the ambient atmosphere.

2.1   EISCAT Svalbard Radar

80 For this study the EISCAT Svalbard Radar (ESR, Wannberg et al. (1997)) in Longyearbyen, Norway (situated at a geographic latitude of 78.15°N and a geographic longitude of 16.02°E and at corrected geomagnetic coordinates of 75.43° and 110.68°) is used. The radar operates at the 500 MHz band and has a 32 m steerable parabolic dish antenna and a 42 m fixed parabolic antenna aligned to the local geomagnetic field. For our purpose, we searched for experiments with good height resolution at D region altitudes. The `manda` experiment (Tjulin, 2017) resolves altitudes of 80 to 100 km with 1–2 km height resolution and
85 was therefore chosen for the radar campaigns in January and February 2019 for this study. In addition to `manda`, all previously run `ipy` experiments were analyzed, as that experiment also covers the mesopause region with a vertical resolution of 4–5 km. The `manda` experiments utilize the 32 m dish and the `ipy` data are collected on the 42 m dish.

2.2 Ebert-Fastie airglow Spectrometer

The Ebert-Fastie spectrometer at the Kjell Henriksen Observatory (KHO) in Longyearbyen, Svalbard, is used to retrieve the
winter temperature of the mesopause (Sigernes et al., 2003). The observatory is located only a kilometer away from the radar
site, so it is practically co-located. The spectrometer scans the near infrared wavelength region, from 824 to 871 nm, which
includes the rotational OH(6–2) band of the OH airglow. The spectrometer points to the zenith with a field of view of 5
degrees. The spectral resolution of the OH(6–2) band is 0.4 nm. One scan of the wavelength range takes 25 seconds but to
obtain a good signal-to-noise ratio several scans are averaged during post-processing of the data. Most earlier studies use 1-
hour averages. In this study, half-hour averaging is used for better temporal resolution. The spectrometer measures whenever
the Sun is more than 12 degrees below the horizon, which at Svalbard latitudes (78.2°N) gives an optical observation season
from the beginning of November until the end of February. The rotational OH temperatures are obtained by fitting a synthetic
spectrum to the measured band of emission lines and using the intensities of four different emission lines of the best fit to
determine the temperature. The details of this procedure are presented in Sigernes et al. (2003). The accuracy of the obtained
rotational temperature is estimated to be ± 2 K. In addition to the fitted temperature values, we use relative band brightness
(non-calibrated arbitrary units) of the P branch of the OH(6–2) transition. These intensity values are routinely calculated and
saved together with the rotational temperatures.

3 Data description and event selection

A total of 10220 hours of ESR data were initially inspected. The `ipy` and `manda` experiment contribute 10144 hours and 76
hours of data respectively. These experiments provide a sufficient height resolution to detect enhanced electron densities at the
mesopause. Here the mesopause region is defined from an altitude of 80 to 100 km to include the hydroxyl (OH) peak height
at 76–90 km (Mulligan et al., 2009). Experiments run in field aligned direction (42m: `ipy`, 32m: `manda`) or vertical pointing
(32m: `manda`) are chosen. The data set starts at the International Polar Year 2007–2008 when the ESR was run continuously
from 1 March 2007 to 29 February 2008 (Blelly et al., 2010). This year includes 8784 hours in the `ipy` experiment mode.
Additionally, all `manda` and `ipy` experiments from December, January and February every year until February 2019 are
included in the analysis. These data span a full solar cycle. The total of 1388 hours of ESR data between 2008–2019 were
analyzed in more detail. Additionally, the ESIRI experiment (ESR Ionospheric D-Region Experiment for Investigation of EPP)
`manda` mode was run for a total of 48 hours in January (24 hours) and February 2019 (another 24 hours) to specifically collect
data for this study. The experiment was run for six evenings between 16 to 22 UT (19 to 01 MLT).

The EISCAT raw data files (Auto-Correlation Functions (ACFs)) are analysed using the GUISDAP data package M. S. Lehti-
nen (1996). This provides an iterative fitting of the ACFs and then, using a model ionosphere, produces the electron densities
examined in this study. The post-integration time is 60 s. Data gaps are shown by white areas in the plots (Figures 1 and 2) and
occur where GUISDAP has not managed to provide a fit. 10-minute averaged electron densities are calculated for the altitude
ranges of 87–90 km and 91–94 km separately. Data from higher than 94 km are excluded. The error of the electron density is
averaged to give a mean error for further analysis.

The search for the EPP events in the radar data is based on an earlier study by Cresswell-Moorcock et al. (2013). The onset is found by a sudden increase of the electron density (median value) by a factor of 5 over 5 minutes. For this study the electron density is averaged to 10 min resolution with an altitude resolution of 4 km. This criterion was slightly adapted to better suit the data from the two different EISCAT experiments. The previous study's factor of 5 was attempted but since there were a

125   number of events just below this acceptance threshold the factor was adjusted to 4. We searched for an increase of electron density by a factor of 4 within 20 minutes from the precipitation onset. If onsets are found only 10 minutes apart, the latter onset is ignored.

The events are detected automatically but inspected and sorted visually based on the temporal evolution of the electron density and the OH temperature. Events with large electron density errors of more than 5×10^9 m^{-3} are excluded. Events

130   which lack more than one temperature measurement within a $\pm$ 3-hour analysis window from the event onset are also excluded. Events which show a particle precipitation signature of electron density enhancement through the whole ionospheric column (87–126 km) are sorted into the EPP category. Events which show an electron density enhancement limited to horizontal layer at the bottom of the E region (around 100 km) are categorized as sporadic E layers (Rapp et al., 2011). The remaining events not showing clear EPP or sporadic E layer behaviour are excluded from the analysis. The sporadic E layer events are not discussed

135   further in this paper. The EPP events with a full coverage of the temperature data, and those only missing one temperature data point are analyzed in more detail. This selection results in a set of eight EPP events, which where categorized into groups of increasing, decreasing and stable (no change) temperature evolution over the EPP onset.

The electron density during the radar run on 6 January from 16:00 UT to 22:00 UT is shown in Figure 1 (top panel). The onset of the EPP is at 19:50 UT and the event lasted until 20:20 UT. The electron density at the lower part of the ionosphere

140   during this experiment was low (mainly below 10^{10} m^{-3}) but abruptly increased at the EPP onset time. The OH rotational temperature (bottom panel) does not change at the event onset. However, it experiences a total decrease of 19 K half an hour after the EPP onset time.

4   Results

Our eight EPP events are listed in Table 1. The criterion for a decreasing or increasing mesopause temperature is that the

145   change has to be larger than the standard deviation (STD) of the temperatures averaged over half an hour. An event is classified as stable (no change), if the temperature change is within the STD of the averaged temperatures.
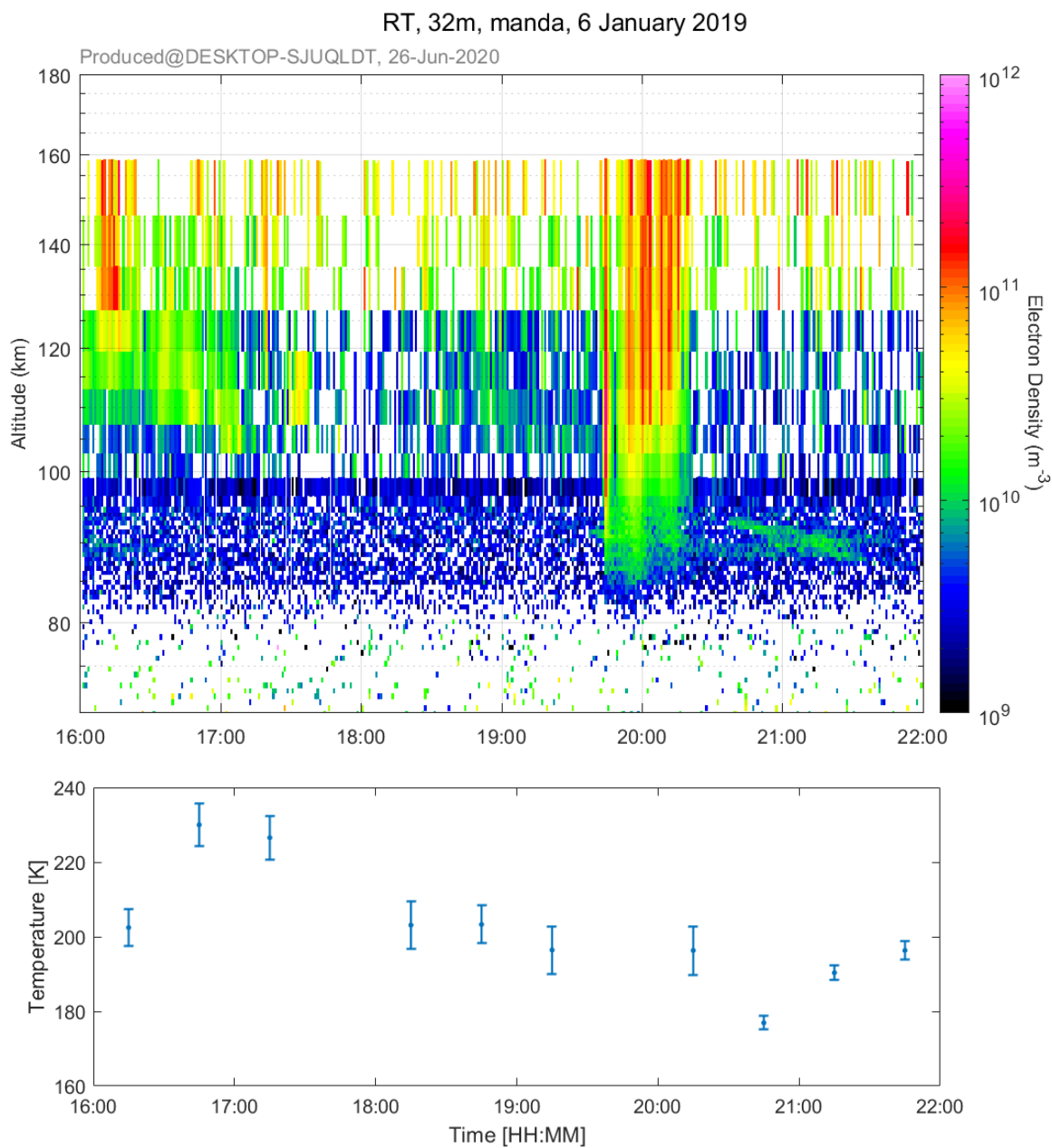
Figure 1. The upper panel shows the electron density as a function of altitude and time for the `manda` experiment on 6 January 2019, at 16:00–22:00 UT. Particle precipitation event found at 19:50 UT. The data are post-integrated to 0.6 km resolution at 80 km height to 3-4 km resolution at 100 km height and 60 s time resolution. The lower panel contains the 30-minute resolution OH temperature data.

#	Event date and time [UT]	T before	T at onset	T after	change in T
1	2007/12/29 23:30	234 [K]	179 [K]	245 [K]	decreasing
2	2008/02/28 02:50	227 [K]	207 [K]	215 [K]	decreasing
3	2011/02/07 22:50	205 [K]	187 [K]	213 [K]	decreasing
4	2013/12/06 21:50	210 [K]	196 [K]	205 [K]	decreasing
5	2014/01/24 02:10	210 [K]	198 [K]	220 [K]	decreasing
6	2014/01/24 15:20	218 [K]	222 [K]	214 [K]	stable
7	2014/01/25 02:40	221 [K]	211 [K]	213 [K]	decreasing
8	2019/01/06 19:50	196 [K]	196 [K]	177 [K]	decreasing

Table 1. Airglow temperature values (degrees in Kelvin in 30 min resolution) before, at and after the event onsets for each EPP event. The last column indicates the observed change in the temperature over the EPP onset.
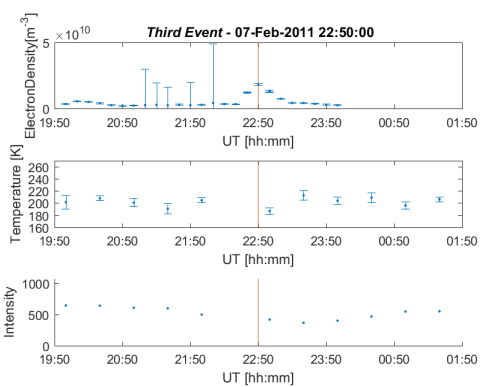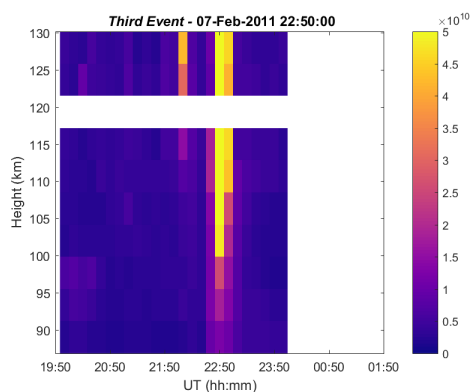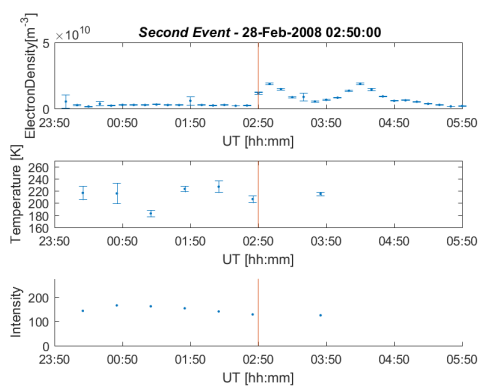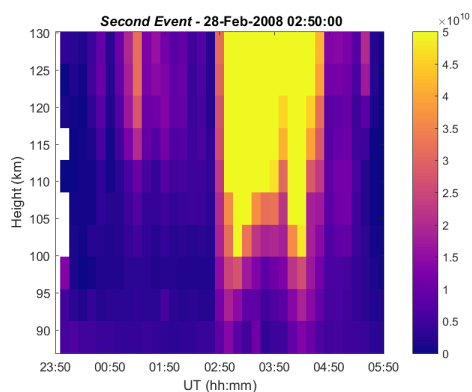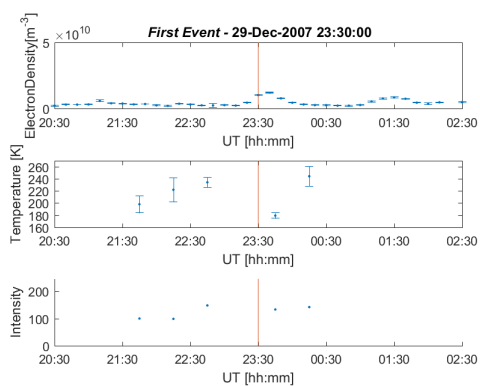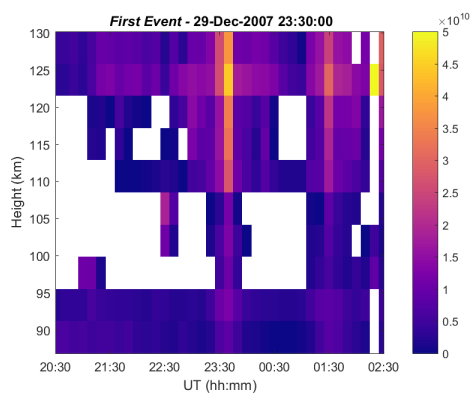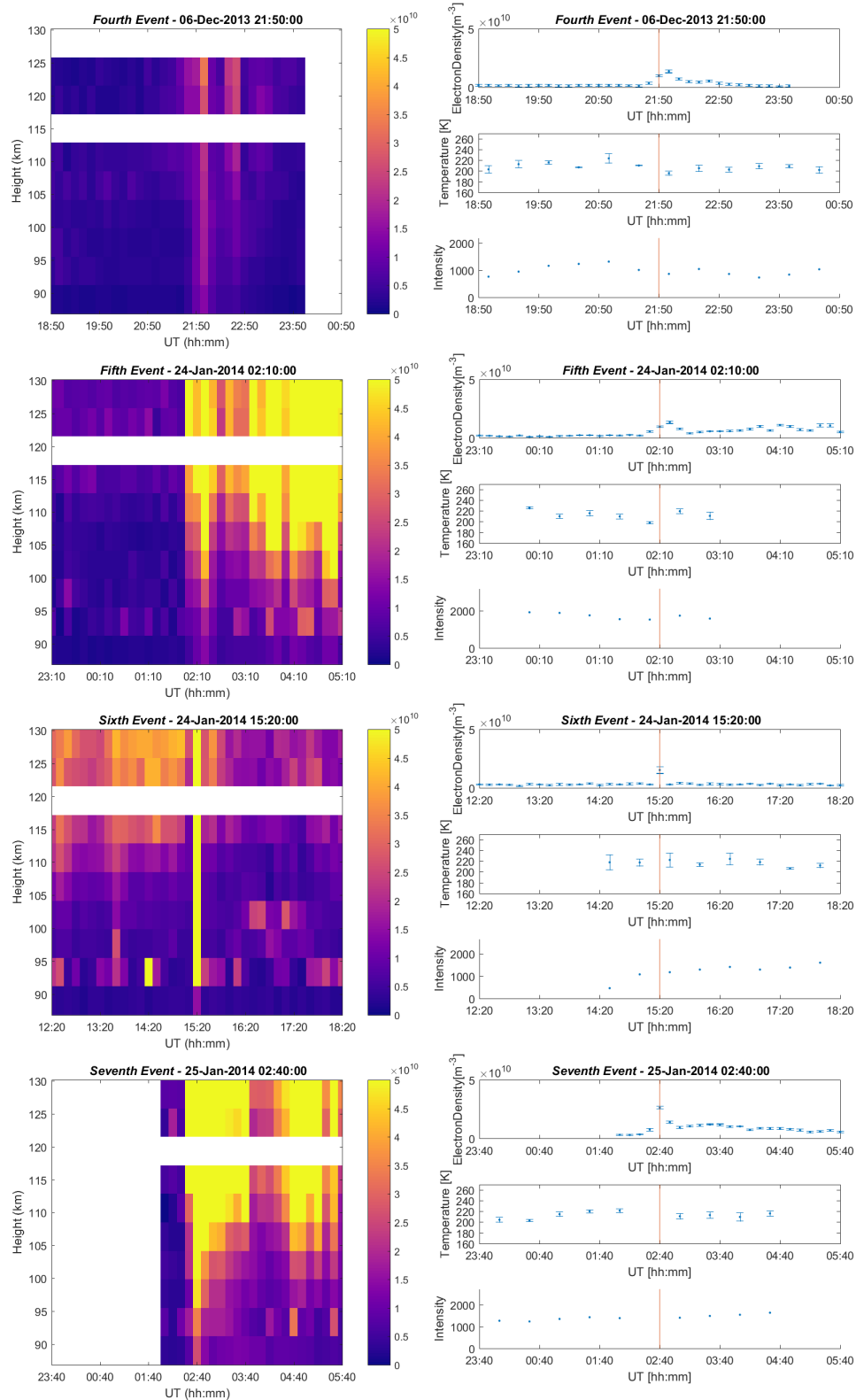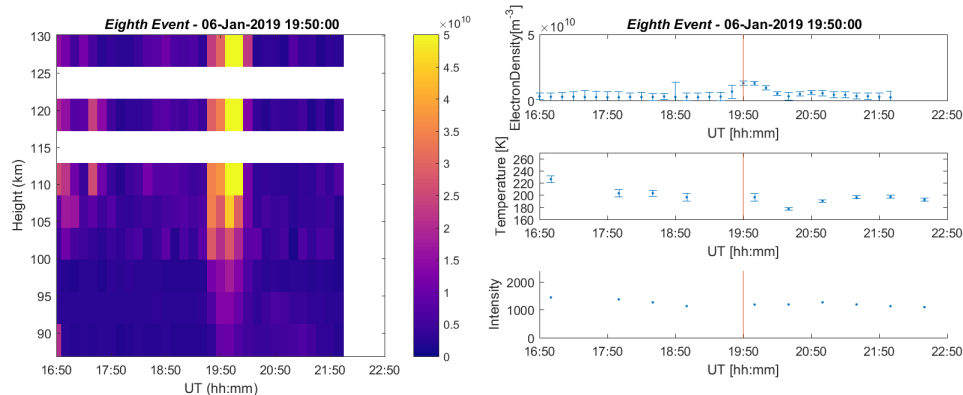
Figure 2. The left column shows the averaged electron density as a function of altitude and time. The right column illustrates the electron density time evolution at the height range where the electron density enhancement was detected. The temporal evolution of the airglow temperature (middle panel) and the relative OH(6–2) band intensity in arbitrary units (bottom panel) are also included. All time axes are given from 3 hours before to 3 hours after the EPP onset, which then takes place in the middle of the plot. The white gaps in the electron density plots indicate missing data.

Figure 2 shows all the EPP events for clarity. The left panels present average electron density as a function of time and altitude, for a 6 hour interval centered at the EPP onset. The right column includes the temporal evolution of the D region electron density (top panel), the airglow temperature (middle panel) and the relative OH(6–2) band intensity (bottom panel).

150   In the line plots the electron densities are from the lowest height range where the increase by a factor 4 was detected. Brief descriptions of each event are given in the following paragraphs.

The first event commences at 23:30 UT on 29 December 2007 and is detected in the altitude range of 91–94 km. The electron density at the EPP event start time is 1.0×10^{10} m^{-3}. The electron precipitation lasts for about 30 min. The mesopause temperature decreases by 55 K (from 234 to 179 K) over the EPP onset time, and recovers within half an hour. The relative

155   OH(6–2) band intensity is 148 before the event and only slightly diminishes to 133 over the EPP onset, but recovers within about 30 minutes similarly to the temperature.

The second event starts at 02:50 UT on 28 February 2008. The electron density enhancement is detected in the height range of 91–94 km with an onset time value of 1.2×10^{10} m^{-3}. The precipitation lasts for about 40 min and is followed by another increase lasting for about 50 min (from 04:00 until 04:50 UT). An airglow temperature decrease of 20 K (from 227 K to

160   207 K) is observed at the EPP onset time. There is only one temperature data point available after the event onset, suggesting an increase of 10 K an hour after the EPP onset. The relative OH(6–2) band intensity decreases gradually from 2 hours before the event until the event onset time. Thus, during this event the intensity behavior is much smoother than that of the temperature. Little or no correlation is seen between the two parameters.

The third event is detected at 22:50 UT on 7 February 2011 at the altitude range of 91–94 km. The electron density at the

165   EPP onset is 1.8×10^{10} m^{-3} and the enhancement lasts for about 30 min. The mesopause temperature decreases from 205 K prior to the EPP to 187 K at the onset time (18°). The minimum temperature is measured at the time of the electron density

maximum. Again, the temperature change recovers within 30 minutes. There is a mild decrease in the relative OH(6–2) band intensity (of 80 arbitrary units) during this event, but the minimum of the emission intensity is reached about half an hour after the temperature minimum, when the temperature and the electron density changes have already recovered.

170   *The fourth event* starts at 21:50 UT on 6 December 2013. It is detected in the altitude range of 87–90 km with an electron density value of 9.9×10^9 m^{-3}. The temperature decreases by 14 K (from 210 to 196 K) over the event onset time. Both temperature and electron density values recover within 30 minutes. The relative band intensity peaks at 1319 an hour before the onset, decreases to 1011 half an hour before the onset and minimizes at 864 at the electron density maximum. A positive correlation between the temperature and band intensity is found in this case.

175   *The fifth event* starts at 02:10 UT on 24 January 2014 at an altitude range of 87–90 km. The electron density at the precipitation onset is 9.5×10^9 m^{-3}, and stays slightly elevated for about two hours after the initial enhancement, which only lasts for about 30 minutes. The mesopause temperature undergoes a decrease of about 12 K, from 210 K prior to the event to 198 K at the EPP onset. The temperature recovery follows that of the initial enhancement in electron density. The OH(6–2) band intensity decreases from 1890 to 1551 already an hour prior to the EPP onset. Similar to the temperature evolution, the

180   emission intensity recovers within half an hour after the onset. There is a mild positive correlation between the temperature and band intensity values.

The sixth event commences at 15:20 UT on 24 January 2014 in the altitude range of 87–90 km. The electron density enhancement is seen in a single profile only (10 min lifetime), with the value of 1.5×10^{10} m^{-3}. The mesopause temperature undergoes mild fluctuations, but all changes are well within the errors and thus, this event is classified as stable. The relative OH

185   band intensity strongly increases (from 460 to 1079) from one hour before to half an hour before the event. After the event onset a more steady and gentle increase in the emission intensity is seen. A more persistent mesospheric electron density enhancement below 95 km may refer to an evolution of sporadic E layer which can affect the temperature evolution. Furthermore, the short lifetime of the electron density enhancement is a good candidate to explain the temperature stability.

The seventh event begins at 02:40 UT on 25 January 2014. It is detected at an altitude range of 87–90 km with an electron

190   density value of 2.6×10^{10} m^{-3}. The electron density enhancement is strong for about 20 min and remains at an elevated level for the next couple of hours. The mesopause temperature undergoes a minor decreases of 10 K (from 221 K to 211 K) over the event onset. The OH band intensity values keep constant with respect to the intensities an hour before the EPP event.

The eighth event starts at 19:50 UT on 6 January 2019 and is detected in the altitude range of 91–94 km. The electron density at the EPP onset is 1.3×10^{10} m^{-3}, and the enhancement lasts for about 30 minutes. The mesopause temperature does

195   not initially decrease when comparing the level before the precipitation to that when the electron density is first enhanced. Nevertheless, there is a decrease of 19 K (from 196 K to 177 K) at about half an hour past the event onset. The relative OH(6–2) band intensity at the event onset is 54 units higher than the level before the event onset time, but stays at a constant level throughout the analysis window.

An overall temperature response to the EPP onsets is shown in Figure 3 by a scatter plot (upper panel) and a superposed

200   epoch analysis (lower panel). The scatter plot includes simultaneous temperature and electron density value pairs around the EPP onset time, from 1 hour before to 2 hours after, for all eight events. The result is an anti-correlation between the electron

density and the airglow temperature with a large range of variation. The average temporal evolution of the temperature response is seen in the superposed epoch analysis from 3 hours before to 3 hours after the precipitation onset. The zero epoch time (EPP onset) shows the lowest temperature both in the median (blue) and the lower percentile (lower red) curves. This immediate
205 temperature decrease is of the order of 10 degrees and recovers within half an hour after the EPP onset. The upper percentile does not show a clear signature of a temperature decrease, which may be due to slightly different timing of the minima as well as the averaging over a time comparable to the temperature change (30 min).

5 Discussion

We have found and analyzed eight electron precipitation events which reached the mesopause and had a good coverage of
210 co-located OH airglow temperature data. Table 1 shows that 7 out of 8 EPP events analyzed in this study were accompanied by a decrease in the mesopause temperature by 10–50 K at the EPP onset. The pre-EPP temperature level (temperature values 1 hour before the event) varied between 196 and 234 K, and the temperature decreased to the range of 177–222 K.

At high latitudes the optical observation season is limited to the four winter months (Nov–Feb). The winter mesopause is characterized by a large temperature variability (of the order of 10 K, Suzuki et al. (2010)) due to gravity wave propagation.
215 It is thus understandable that there is no consensus of the temperature response to the energetic particle precipitation when any minor change is likely to be lost in the highly variable background conditions. The temperature responses found in this study, however, are larger than 10 degrees. The short lifetime (∼30 minutes) of the observed temperature responses does not allow this signature to be detected in any analysis utilizing hourly or daily averaged temperature data. For instance, the fast temperature decrease and equally quick recovery shown by the superposed epoch analysis (bottom panel of Figure 3) would
220 not be a significant change in hourly or daily averaged epoch.

The first event at 23:30 UT on 29 December 2007 (top panel of Figure 2) shows a strong decrease in the mesopause temperature at the time of the EPP onset. Similarly, in *the third* and *fourth events* (at 22:50 UT on 7 February 2011, and at 21:50 UT on 6 December 2013) a very quiet ionospheric conditions (low electron density) are seen prior to the EPP onset, and the connection between the electron density enhancements and the temperature changes is particularly clear. This is a typical behavior
225 in our set of events. It is further demonstrated by the anti-correlation between the airglow temperature and the electron density seen in the top panel of Figure 3.

The lifetime of the EPP events in this study is typically 20–50 minutes, and the corresponding neutral temperature response is equally short. In *the second*, *fifth*, and *seventh event* the short-lasting electron density enhancements are followed by longer lasting but gently elevated levels of electron densities. In all these cases the electron fluxes reaching the E region heights (above
230 100 km) are high for a couple of hours after the EPP event, but only at the very beginning of the precipitation event did they reach the altitudes below 100 km. Consequently, the temperature behaviour is smooth and steady apart from the short-term change around the EPP onset.

Our *sixth event* (at 15:20 UT on 24 January 2014) was classified as stable in terms of the mesospheric temperature response. The electron density increase in this event has the shortest lifetime of all our events, as it is seen in one 10-min profile only.

235   The lifetime of the electron bombardment may thus be the key factor determining whether a measurable neutral temperature response is seen.

A statistical study on high-latitude OH airglow temperatures and emission intensities by Shepherd et al. (2007) shows a strong positive correlation between the two parameters in the time scales from hours to seasons. This is explained by vertical motion of the airglow layer driven by atmospheric dynamics. For instance, as an airglow layer undergoes downward motion

240   the adiabatic heating increases its temperature. The lower peak emission height coincides with higher mixing ratio of oxygen and therefore, enhances the production of the excited OH. The temperature changes observed in our study typically take place in shorter time scales. The correlation between the OH(6–2) temperature and the relative band intensity of 30-minute averaged data can be visually inspected in Figure 3. While a positive correlation can be seen between the two parameters in case of the *fourth* and *fifth* event, no significant correlation across the entire event set was found (data not shown).

245   An increase in the mesospheric temperature during particle precipitation would agree with the Joule heating effect suggested by earlier studies (Nesse Tyssøy et al., 2010). In fact, a temperature increase of about 10 K was observed in the study by Suzuki et al. (2010). In our study, however, it was found that the mesopause temperature typically responds to the particle impact with a decrease of about 20 K. A way to explain the temperature change Suzuki et al. (2010) discussed was that the EPP ionisation changes the mesospheric chemical composition by decreasing the population of excited OH at the top of the

250   layer. As a consequence, the peak height of the airglow changes and the temperatures are probed at lower altitudes than before. It was suggested that the energetic electron impact can dissociate oxygen and ozone molecules (Maeda, 1967). When less O_3 is available, less excited OH molecules are produced as ozone is a key ingredient in the production of excited hydroxyl:

$$H + O_3 \rightarrow O_2 + OH^*(v' \leq 9), \tag{1}$$

where v' corresponds to the upper vibrational level of the OH molecule, which in our case is 6. The dissociation of molecular

255   oxygen and ozone by energetic electrons can therefore lead to a decrease in the emission of the OH airglow. The fitted rotational OH temperature corresponds to the average height of the airglow layer. The peak is assumed to be at about 87 km. If, however, the production of excited OH is temporarily prohibited at the top part of the airglow layer, the temperature will then represent the layer, which is now centered at lower heights. Depending on the local gradient in the mesospheric temperature profile, this may lead to increased or decreased temperature value. In this scenario, the relative OH(6–2) band intensity would decrease as

260   the airglow layer becomes thinner, which is true for most of the events analyzed in this study. In particular at the top of the mesosphere the temperature can vary on the order of 10 K over a height range of a few kilometers. Even if the temperature change produced in this scenario is of the right order of magnitude, it is interesting that all EPP events analyzed in this study, which did cause a temperature change, showed a decrease. Our results together with the previous results by Suzuki et al. (2010) present an inconsistent temperature response to EPP. Therefore, a larger number of events should be collected and

265   examined to conclude if the OH airglow layer favors a height region with a positive temperature gradient upwards. Furthermore, an immediate temperature response and its fast recovery suggests that the longer-term and larger-scale heat balance in the mesosphere is little affected by EPP, unless the actual precipitation has a substantial lifetime (hours to days).

6   Conclusions

A total of 10220 hours of electron density measurements were browsed in the search of enhancements due to energetic elec-
270   tron precipitation (EPP) events with simultaneous temperature calculations from OH airglow measurements. A total of eight
events of electron density enhancements were found and analyzed in this study. We investigated the existence of any coherent
behaviour between the electron density enhancements at the D region heights and the mesopause temperature. The response
of the mesopause temperature on the EPP energy deposition is predominately (7 out of 8 events) an immediate decrease of
10–50 K, which recovers within 30 to 60 minutes after the EPP onset. The temperature decrease found in this study, together
275   with a temperature increase in a previous study is interpreted as an EPP ionisation decreasing the production of the excited
OH at the top of the airglow layer. As a consequence, the airglow layer becomes thinner, the peak height is reduced and the
airglow temperatures correspond to lower altitudes. Investigating the change in the relative OH(6–2) band intensity shows a
decrease during the majority of our EPP events and thus supports the thinning scenario as a valid mechanism for changing
the measured temperature. Furthermore, the relative OH brightness values are only poorly correlated with the temperatures
280   in the time scales of a few hours, which is not in agreement with purely dynamically driven temperature changes. Given the
short-lived characteristic of atmospheric temperature change, EPP may not have climate effects except for long-lasting events.

Data availability.   The temperature data are available as quicklooks plots online at kho.unis.no. The Eiscat Svalbard Radar data have been
downloaded from https://eiscat.se and are the intellectual property of the EISCAT Scientific Association. The EISCAT raw data files are
analyzed by using the Grand Unified Incoherent Scatter Design and Analysis Package (GUISDAP) M. S. Lehtinen (1996)

285   .

Author contributions.   Florine Enengl carried out the analysis of the data and the writing of the paper. Noora Partamies proposed the idea
of the study, fitted and pre-analyzed the airglow temperature data, shared her expertise and together with Nickolay Ivchenko took part in
the discussions, interpretations, planning and structure of the work. Lisa Baddeley advised and helped describing and analysing the EISCAT
data. All co-authors helped in the writing process with comments, suggestions and edits on the paper.

290   *Competing interests.*   No competing interests are present.

Disclaimer.   The data and figures have been used in the MSc thesis by F. Enengl, available through http://kth.diva-portal.org/

Acknowledgements. The work by NP & LB is supported by the Research Council of Norway (NRC) under CoE contract 223252, and NP is further supported by the NRC contract 287427. The authors thank Fred Sigernes and Mikko Syrjäsuo for the maintenance of the OH airglow spectrometer. EISCAT is an international association supported by research organisations in China (CRIRP), Finland (SA), Japan (NIPR and ISEE), Norway (NFR), Sweden (VR), and the United Kingdom (UKRI). The authors thank Ingemar Häggström for his assistance with the EISCAT data.

295

References

Andrews, D. G.: An Introduction to Atmospheric Physics Second Edition, CAMBRIDGE UNIVERSITY PRESS, 2010.

Blelly, P. L., Alcaydé, D., and van Eyken, A. P.: A new analysis method for determining polar ionosphere and upper atmosphere characteristics from ESR data: Illustration with IPY period, Journal of Geophysical Research (Space Physics), 115, A09322, https://doi.org/10.1029/2009JA014876, 2010.

Cho, Y. nd Shepherd, G. G.: Correlation of airglow temperature and emission rate at Resolute Bay (74.68°N), over four winters (2001–2005, Geophysical Research Letters, 33, n/a–n/a, 2006.

Cresswell-Moorcock, K., Rodger, C. J., Kero, A., Collier, A. B., Clilverd, M. A., Haggstrom, I., and Pitkanen, T.: A reexamination of latitudinal limits of substorm-produced energetic electron precipitation, Journal of Geophysical Research. Space Physics, 118, 6694–6705, https://doi.org/10.1002/jgra.50598, 2013.

Gavrilyeva, G. and Ammosov, P.: Influence of geomagnetic activity on mesopause temperature over Yakutia, Atmospheric Chemistry and Physics, 18, 3363–3367, https://doi.org/10.5194/acp-18-3363-2018, 2018.

Holmen, S., Dyrland, M., and Sigernes, F.: Mesospheric temperatures derived from three decades of hydroxyl airglow measurements from Longyearbyen, Svalbard (78 N), Acta Geophysica, 62, 302–315, https://doi.org/10.1029/2001JA009023, 2014.

M. S. Lehtinen, A. Huuskonen, J. P.: First experiences of full-profile analysis with GUISDAP, Annales Geophysicae, European Geosciences Union, pp. 1487–1495, https://doi.org/10.1007/s00585-996-1487-3, 1996.

Maeda, K.: The auroral O2-dissociation and the infrared OH-emission, Tech. rep., http://hdl.handle.net/2060/19670030065, 1967.

Mulligan, F., E. Dyrland, M., F, S., and S. Deehr, C.: Inferring hydroxyl layer peak heights from ground-based measurements of OH(6-2) band integrated emission rate at Longyearbyen (78 N, 16 E), Annales Geophysicae, 27, https://doi.org/10.5194/angeo-27-4197-2009, 2009.

Nesse Tyssøy, H., Stadsnes, J., Sørbø, M., Mertens, C. J., and Evans, D. S.: Changes in upper mesospheric and lower thermospheric temperatures caused by energetic particle precipitation, Journal of Geophysical Research: Space Physics, 115, https://doi.org/10.1029/2010JA015427, 2010.

Rapp, M., Leitert, L., Latteck, R., Zecha, M., Hoffmann, P., Höffner, J., Hoppe, U., La Hoz, C., and Thrane, E. V.: Localized mesosphere-stratosphere-troposphere radar echoes from the E region at 69°N: Properties and physical mechanisms, Journal of Geophysical Research: Space Physics, 116, n/a–n/a, 2011.

Shepherd, G., Cho, Y.-M., and Liu, G.: Correlations of mesospheric variability ad their relation to the large-scale circulation during polar winter, Journal of Atmospheric and Solar-Terrestrial Physics, 69, 2279–2291, https://doi.org/10.1016/j.jastp.2007.06.007, 2007.

Sigernes, F., Shumilov, N., Deehr, C. S., Nielsen, K. P., Svenøe, T., and Havnes, O.: Hydroxyl rotational temperature record from the auroral station in Adventdalen, Svalbard (78N, 15E), Journal of Geophysical Research: Space Physics, 108, https://doi.org//10.1029/2001JA009023, 2003.

Suzuki, H., Tsutsumi, M., Nakamura, T., and Taguchi, M.: The increase in OH rotational temperature during an active aurora event, Annales Geophysicae, 28, 705–710, https://doi.org/10.5194/angeo-28-705-2010, https://www.ann-geophys.net/28/705/2010/, 2010.

Tjulin, A.: EISCAT experiments, https://www.eiscat.se/wp-content/uploads/2016/05/Experiments.pdf, 2017.

Wannberg, G., Wolf, I., Vanhainen, L. G., Koskenniemi, K., RöTtger, J., Postila, M., Markkanen, J., Jacobsen, R., Stenberg, A., Larsen, R., Eliassen, S., Heck, S., and Huuskonen, A.: The EISCAT Svalbard radar: A case study in modern incoherent scatter radar system design, Radio Science, 32, 2283–2307, https://doi.org/10.1029/97RS01803, 1997.
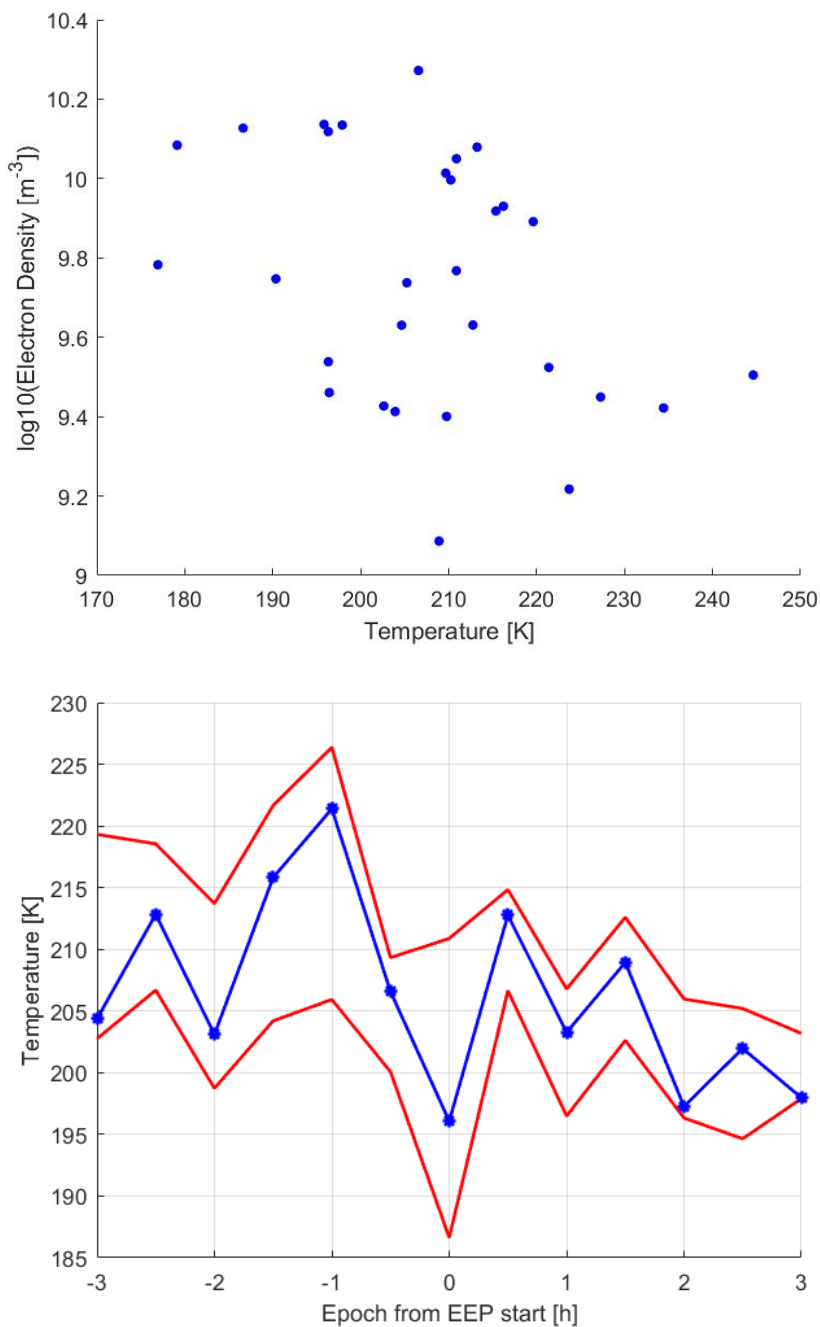
Figure 3. This figure illustrates the average temperature response to the EPP onset. The upper panel shows a scatter plot of the electron density and the airglow temperature values (before, at and after the EPP onset). The superposed epoch of the airglow temperature (lower panel) includes the 25% (lower red line), 50% (blue) and 75% (upper red line) percentiles of the temperature for all eight events. The zero epoch time corresponds to the EPP onset. Each 30 min epoch time bin contains 3–7 temperature values, maximizing around the zero epoch time.